Transistors platform for rapid and parallel detection of multiple pathogens by nanoscale-localized multiplexed biological activation

Elisa Riedo

elisa.riedo@nyu.edu

New York University https://orcid.org/0000-0002-2423-8801

Alexander Wright

New York University https://orcid.org/0000-0002-9267-5552

Hashem Nasralla

New York University

Rahul Deshmukh

New York University

Moeid Jamalzadeh

New York University

Matthew Hannigan

New York University

Andrew Patera

SUNY Downstate Health Sciences University

Yanxiao Li

New York University

Miguel Manzo-Perez

New York University

Nitika Parashar

Tandon School of Engineering, New York University

Zhujun Huang

New York University

Thanuka Udumulla

Mirimus

Weiqiang Chen

New York University https://orcid.org/0000-0002-9469-8328

Davide de Forni

ViroStatics srl.

Marcus Weck

New York University

Giuseppe de Peppo

Mirimus Inc.

Davood Shahrjerdi

New York University https://orcid.org/0000-0002-5955-1830

Article

Keywords:

Posted Date: January 26th, 2024

DOI: https://doi.org/10.21203/rs.3.rs-3810461/v1

Additional Declarations: There is **NO** Competing Interest.

Abstract

The rise in antibiotic-resistant pathogens, highly infectious viruses, and chronic diseases has prompted the search for rapid and versatile medical tests that can be performed by the patient. An electronic biosensing platform based on field-effect transistors (FETs) is particularly attractive due to sensitivity, fast turn-around, and compatibility with semiconductor manufacturing. However, the lack of methods for pathogen-specific functionalization of individual FETs prevents parallel detection of multiple pathogens. Indeed, so far functionalization of FET based biosensors is achieved by drop casting without any spatial selectivity. Here, we propose a paradigm shift in FET's biofunctionalization. Specifically, we use thermal scanning probe lithography (tSPL) with a thermochemically sensitive polymer that can be spin-coated on any FET material. We demonstrate that this scalable, CMOS compatible methodology can be used to functionalize individual FETs with different bioreceptors on the same chip, at sub-20 nm resolution, paving the way for massively parallel FET detection of multiple pathogens. Antibody- and aptamer-modified FET sensors are then realized, achieving an ultra-sensitive detection of 5 aM of SARS-CoV-2 spike proteins and 10 human SARS-CoV-2 infectious live virus particles/ml, and selectivity against human influenza A (H1N1) live virus.

Introduction

A variety of global health threats, such as highly infectious viruses, chronic diseases, and increasing prevalence of antibiotics-resistant pathogens, require rapid and versatile tests which can be performed by the patient. Field-effect transistors (FETs) configured as biosensors serve as a suitable platform, compatible with modern semiconductor manufacturing, for label-free rapid sensing by converting interactions between target analytes and surfaces into real-time electrical signals [1–4].

However, the application of FET-based sensors for highly parallel detection of multiple distinct pathogens or biomarkers remains elusive. At present, functionalization of FET based biosensors is achieved by drop casting without any spatial selectivity. Therefore a critical need is a CMOS-compatible and scalable surface chemistry fabrication strategy that can allow modification of each FET on a chip on-demand with distinct pathogen/biomarker-specific bioreceptors, such as antibodies [5, 6] and aptamers [7, 8]. Overcoming this challenge will enable portable and wearable rapid diagnostic tests with unprecedented capabilities.

Furthermore, the detection limits of FET-based sensors have been pushed to ultralow concentrations (i.e., femto-molar or less) by adapting nanoscale materials such as nanowires [9, 10], In_2O_3 [7], and graphene [11–13]. The progress in this direction promises new applications for FET-based sensor technologies in drug discovery [14, 15] and clinical diagnostics [16–19]. Nonetheless, existing surface functionalization strategies have several limitations. A primary limitation is the lack of a spatially selective methodology with nanoscale precision for realizing bioreceptor-modified FET sensors. The proposed approach so far to achieve multiplexing is to create physical macroscopic barriers between different FETs [7, 12, 20], using for example polydimethylsiloxane (PDMS) barriers and chambers measuring several millimeters in size

(see Supplementary Table 1 for a review). However, modern semiconductor manufacturing can integrate billions of sub-100 nm size FETs into functional microchip products [21], therefore, a paradigm shift in biofunctionalization is required for configuring each individual nanoscale FET into a distinct pathogen/biomarker-specific biosensor.

Another limitation pertains to the development of surface chemistry processes that are FET-material independent. For instance, attaching a given antibody or aptamer to a graphene film will involve different processing steps compared to an oxide film. Functionalizing graphene requires creating either ester or vinyl sulfone groups on the surface [22], which react with the primary amine groups of the receptor-antibodies. On the other hand, a different approach is needed for functionalizing In_2O_3 FETs sensors with aptamers, involving the covalent modification of In_2O_3 with dopamine or serotonin aptamers using silane chemistry [7]. These functionalization strategies depend on the FET material and lack the ability to allow local chemical patterning of each FET with a different bioreceptor, as the entire biosensor chip is functionalized identically.

To address the above-mentioned limitations, here, we introduce a scalable, CMOS compatible functionalization strategy, applicable to any FET material, permitting local chemical modification of individual nanoscale FETs on the same chip with different bioreceptors from antibodies to aptamers, at sub-20 nm resolution and 200 nm pitch, a distance comparable to the pitch of modern FETs array in CMOS chip. Our strategy involves the use of thermal scanning probe lithography (tSPL) with a thermochemically sensitive polymer. We demonstrate the capability of this strategy through multiplexed functionalization with different bioreceptors at nanoscale precision. In a typical FET biosensor, the detection occurs by recording the change in charge near the channel region, due to the trapping of a target analyte by a specific bioreceptor. We show that changes in charge at the surface of the polymer covering the FET channel equally give rise to detectable electronic signals by capacitively coupling through the polymer film. Furthermore, the ability to pattern individual FET allows for *in-situ* differential sensing, a key ingredient to ensure signal fidelity. The feasibility of this platform is established by testing antibody- and aptamer-modified FET sensors fabricated using this polymer-based FET biofunctionalization approach. The sensors achieve an ultra-sensitive detection of 5 aM of SARS-CoV-2 spike proteins and 10 human SARS-CoV-2 infectious virus particles/ml, which caused the COVID-19 pandemic, and selectivity against human influenza A (H1N1) live virus.

Results and Discussion

Nanoscale thermal biofunctionalization: the NanoBioFET platform

To implement a scalable strategy capable of locally functionalizing individual FETs at sub-100 nm resolution with desired bioreceptors (from antibodies to aptamers), and applicable to any channel material (e.g., graphene, oxides or silicon), we use thermal scanning probe lithography (tSPL) [23, 24]. In our approach, tSPL uses a hot nanotip to expose amine groups with nanoscale resolution on a thermally sensitive biocompatible polymer resist [25–29], which is spin coated on a fully-fabricated array of FETs

(see Fig. 1b). This spatially selective activation process enables subsequent modification of individual or a group of FETs with a desired bioreceptor, resulting in an array of FET-based biosensors configured for simultaneously detecting various target analytes (see Fig. 1a). We name this platform NanoBioFET.

The implementation of the NanoBioFET platform begins by fabricating a FET array. As shown in Fig. 1b, we adopt monolayer graphene for realizing the FET-based sensors (see Methods), due to its potential for ultrahigh sensitivity [30, 31]. We then cover the fully fabricated graphene FETs (gFETs) by spin coating two thermally sensitive polymer resist films (see Methods). The stack comprises a first film of about 70-nm-thick polymethacrylate-carbamate-cinnamate copolymer (PMCC) [26–28], which provides amine groups on demand in designated FET regions upon local heating by tSPL. PMCC can be locally patterned through local heat-induced deprotection of amine groups from tetrahydropyranyl carbamates in the carbamate block of PMCC [25–29] (see Methods). The second film is poly(phthalaldehyde) (PPA) [23, 32] which serves as a top layer resist (10–20 nm thick) to reduce non-specific binding outside the FET channel region (see Supplementary Note 1).

After forming the bilayer polymer resist stack, we proceed with the localized functionalization of individual FETs with desired bioreceptors. Employing tSPL, we modify the bilayer polymer resist stack atop the channel region of each target gFET with amine groups. This process utilizes a hot nano-tip in a commercial tSPL system (see Methods), which removes PPA completely above the channel region, while simultaneously applying heat to the PMCC polymer surface above the amine deprotection temperature (~ 120 C), exposing amine groups in the desired area (Fig. 1b). For differential sensing, we pattern only the FET used as a sensor, while leaving un-patterned the FET used as a control. Ensuring signal fidelity is a key challenge for commercialization of FET-based biosensors. Hence, providing a platform that allows for *in-situ* differential sensing is a key milestone. Using standard conjugation strategies, the amine groups in the channel region can subsequentially be functionalized with ad-hoc bioreceptors such as antibodies or aptamers (see Methods for details). At this point, the sensor/control FETs are ready for biodetection of a specific target, such as SARS-CoV-2 virus. As discussed later, when the FET sensor is exposed to a specific target, the target is immobilized by the bioreceptor near the polymer surface, giving rise to a change in the electronic signal of FET-based sensors.

In Fig. 1c, we demonstrate the resolution of the NanoBioFET fabrication method. Specifically, Fig. 1c shows an *in-situ* tSPL topographical image (see Methods) of an amine pattern produced by tSPL in a PPA/PMCC bilayer polymer resist stack deposited on a SiO_2/Si wafer (without graphene). The pattern consists of a 10 x 10 matrix of 15 nm-diameter amine circles with 40 nm pitch. This image shows a resolution compatible with the 5 nm-node silicon FET technology and below. Importantly, this image is taken *in-situ* during the tSPL patterning process, since thermal probes can also allow local nanoscale imaging (Methods). This feature enables localization of target regions on a chip with nanoscale precision without requiring sophisticated and costly pattern alignment procedures.

To demonstrate the ability of the NanoBioFET fabrication method to pattern relevant biomarkers with high reproducibility and precision, Figs. 1d and 1e present two fluorescence optical microscopy images of

one-hundred squares (with 5 μm and 500 nm sides, respectively) of biotinylated anti-SARS-CoV-2 aptamers, which have been fluorescently tagged with a red dye (see Methods for details on the aptamers used here). These aptamer patterns have been produced first by exposing amine groups by tSPL on the surface of the PPA/PMCC polymer resist, and then by conjugating the amine groups to NHS-biotin, followed by streptavidin, and biotinylated aptamers (the details of the chemical functionalization steps are reported in the Methods). The PPA/PMCC double polymer stack is here spin-coated on a silicon oxide/silicon wafer.

In Figs. 1f and g, we show how the NanoBioFET fabrication process is implemented on a gFET array chip. For this purpose, we fabricate an array of four gFETs with a channel length of 1 μm, where each sensor FET is adjacent to a control FET. The PPA and PMCC resists are then spin-coated on the gFETs, and tSPL is used to remove PPA and pattern amine groups in the channel region of the two gFET sensors, leaving the FET controls unpatterned. In Figs. 1f and g we show, respectively, an *in-situ* tSPL topographical image, and an *ex-situ* friction atomic force microscopy (AFM) image of the resulting gFET sensors and controls after tSPL patterning. The graphene region underneath the polymer is indicated with a dashed red rectangle. In Fig. 1f, the tSPL topography image shows that the patterns above the channel region of the gFET sensors are at a depth of approximately 10 nm, corresponding to the thickness of the PPA film, which is sublimated during tSPL patterning. It is important to note that since tSPL allows *in-situ* imaging of the FET underneath the dual polymer stack, we are able to locate the channel region of each FET and pattern where required without the need of markers. The AFM friction image in Fig. 1g is particularly revealing since it shows clear friction contrast in the sensor area due to the change in hydrophilicity upon the thermal deprotection of the amine moiety. This agrees with a more hydrophilic surface where the amine groups have been exposed, and the consequent presence of larger friction forces at the nanoscale due to larger capillary forces [24, 33].

The NanoBioFET platform for parallel biochemical sensing

To fully exploit the potential of having a massive number of FET biosensors in a microchip, it is necessary to functionalize each FET with distinct bioreceptors so as to allow detection of different types of target biomolecules, such as different viruses. In Fig. 2, we demonstrate the capability of the NanoBioFET fabrication process to pattern each FET with an independent bioreceptor to permit parallel sensing on the same chip. Figure 2a shows a schematic representing the steps required for patterning the different FETs with distinct bioreceptors. Initially, we fabricate an array of FETs and we spin-coat a PPA/PMCC polymer stack on them. Then a first round of NanoBioFET fabrication, as depicted in Fig. 1b, is performed on FET-1 to attach bioreceptor-1 (red square), followed by a second round to attach bioreceptor-2 (green square) to FET-2, and so on until all FETs are functionalized up to the desired n-number of bioreceptors. Each round of NanoBioFET fabrication includes: first, *in-situ* tSPL topographical imaging of the surface to locate where the pattern needs to be made (e.g., the desired FET); second, tSPL local patterning of an individual FET channel; third, a series of biochemical functionalization steps, and selective attachment of the desired bioreceptor to the required FET as described in the Methods part.

In Fig. 2b we present a fluorescence optical microscopy image of biochemical patterns generated by four sequential rounds of NanoBioFET fabrication as depicted in Fig. 2a. In particular, Fig. 2b shows the fluorescence of four types of NHS-esters terminated dyes (red, yellow, green and sky-blue) attached directly to the amine moieties exposed during the tSPL process on the surface of the PPA/PMCC polymer resist deposited on a silicon oxide/Si wafer. Figure 2c shows the implementation of the multiplexed chemical patterning in an array of gFETs. Specifically, four representative gFETs channel regions have been functionalized with four different types of NHS-esters terminated dyes (red, yellow, green, and sky-blue) attached directly to the amine moieties exposed by tSPL on the surface of a PPA/PMCC polymer resist spin-coated on a gFET chip.

Figures 2d and e demonstrate the capability of the NanoBioFET fabrication method to produce independent patterns of different types of bioreceptors sensitive to different types of target molecules, e.g., different viruses. In particular, here we show a fluorescence image of patterns of two types of fluorescently labelled aptamers, influenza A anti-hemagglutinin (HA) aptamer tagged with a green fluorophore, and anti-SARS-CoV-2 aptamer (tagged with a red fluorophore). The patterns are created by exposing amine groups by tSPL, and subsequently by attaching NHS-ester biotin to the amine patterns. Biotin patterns are then exposed to streptavidin, and finally to the biotinylated HA aptamer (green). A second identical round of NanoBioFET fabrication is performed to attach the biotinylated CoV-2 aptamer (red) to the desired area on the surface. The details are reported in the Methods.

Figures 2e and f demonstrate the high spatial resolution with which patterns/bits of different bioreceptors can be fabricated on the channel of parallel FETs with this approach. In particular, following the same process as in Figs. 2d and e, we produce patterns of two types of aptamers (HA and CoV-2 aptamers). The fluorescence image in Fig. 2e shows green-aptamer and red-aptamer patterns with a “bit” dimension of 500 nm. Because of the limited resolution offered by optical microscopy, we also fabricate two-aptamer circle/dash patterns with a 20 nm width and a minimum 200 nm pitch, i.e., minimum distance between circle (HA aptamer) and dash (CoV-2 aptamer) pattern centers. We then image them *in-situ* by tSPL imaging (Fig. 2f). We perform three measurements on the PPA/PMCC surface. First, we image pattern type-circle after a first round of tSPL. Second, we functionalize pattern type-circle with NHS-biotin/streptavidin/HA aptamer and image the pattern region after a second round of tSPL to produce pattern type-dash. Third, we image the polymer surface after functionalization of pattern type-dash with NHS-biotin/streptavidin/CoV-2 aptamer. The cross-sections show the high registry and robustness of the fabrication process and the change in depth of the patterns after functionalization due to the filling of each pattern with the NHS-biotin/streptavidin/aptamer molecules (approximately 10–15 nm). The two types of patterns have been produced with different shapes to add clarity to the image and show that tSPL can also produce patterns at different depths and shape. See also supplementary Figure S8.

Electronic sensing using the NanoBioFET platform

Having established the versatility and nanoscale spatial precision of the NanoBioFET fabrication strategy, we next examine its feasibility in electronic detection of target analytes. As a proof-of-concept, we implement electronic sensors based on gFETs. Our sensing experiments are tailored for the detection of the SARS-CoV-2 virus, chosen as an example target species. This choice is motivated by the commercial availability of bioreceptors for this virus, including different antibodies and aptamers.

gFETs are promising biosensor candidates due to their potential for high sensitivity and ease of fabrication [13, 22, 34]. Like other FET-based biosensors, a bioreceptor-modified gFET translates the pathogen-bioreceptor interaction near the surface to a detectable electronic signal. Figure 3a shows the schematic illustration of an antibody-modified gFET. The sensor is solution-gated, where a fixed bias gate voltage (V_{gs}) is applied to the solution (300 mV in our experiments) using a Ag/AgCl reference electrode. A small bias voltage (V_{ds}=50 mV) is simultaneously applied between the source and drain electrodes, generating a current flow (I_{ds}) in the gFET, which is monitored in real time. The amplitude of I_{ds} changes upon conjugation of target analytes (e.g., spike protein or virus) with bioreceptors, due to a change in electronic charge on the surface of the biosensor. Furthermore, the recorded I_{ds} signal can be used to quantify the concentration of target analytes through creation of a sensitivity calibration curve, as we explain later.

However, a key experimental challenge in FET-based biosensing is the electronic screening of charges with increasing distance from the surface, characterized by the Debye length λ_{Debye}. A common approach for overcoming this limitation is to adjust the ionic strength of the buffer environment [35, 36], thereby increasing λ_{Debye}. In the experiments below, we adopt a similar strategy, modifying the buffer solution and its ionic strength based on the choice of the bioreceptor (i.e., antibody or aptamer).

Sensing using antibody-modified NanoBioFET

All electronic sensing experiments begin by employing the fabrication and biofunctionalization protocols described in Figs. 1 and 2, which involve anchoring NHS-biotin-streptavidin chains onto the thermochemically activated amine groups on the PMCC polymer, above the channel region of the gFETs. Our initial investigations focus on the use of biotinylated antibodies as a bioreceptor, which attach to the NHS-biotin-streptavidin chains. In this configuration, detecting an electronic signal induced by the antibody-analyte interaction requires λ_{Debye} of at least ~ 10 nm. To accommodate this requirement, we use a 1 mM HEPES buffer solution as the sensing environment (see Methods) [9]. Whereas a lower ionic strength enhances λ_{Debye}, the reduction of ion concentration in the sensing environment may negatively affect the efficacy of the antibody-analyte interaction.

We select biotinylated anti-SARS-CoV-2 spike RBD neutralizing antibody (see Methods) for these electronic sensing experiments. The feasibility of its binding affinity to SARS CoV-2 spike protein at 1mM HEPES buffer is confirmed by surface plasmon resonance (SPR) measurements (Fig. 3b). In these SPR experiments, the concentration of spike proteins is limited to a low nanomolar range, which is the typical sensitivity of this type of measurements [37, 38]. Following this confirmation, we proceed to perform the

electronic sensing measurements with the NanoBioFET platform. In all sensing experiments, the bioreceptor-modified gFETs are placed in a microfluidic chamber (see Methods). We then perform an initial screening of a gFET sensor quality by measuring its transfer characteristics (I_{ds} vs. V_{gs}) using a buffer solution gate. In Fig. 3c, we show the typical transfer characteristics of an antibody-modified gFET, obtained by sweeping the solution gate voltage, V_{gs}, and recording I_{ds} at a fixed V_{ds} of 50 mV. V_{gs} modulates the gFET charge carrier concentration and carrier type, from holes in the p-branch, to electrons in the n-branch, passing through the charge neutrality point (at V_{CNP}). For simplicity the data are centered around V_{CNP}. When an analyte is captured by the bioreceptor in the channel region, the local change in charge produces a shift of the I_{ds} vs.V_{gs} characteristics and therefore a change in I_{ds} is measured at fixed V_g.

We next monitor the real-time electronic response of a SARS-CoV-2 antibody-modified gFET sensor to different concentrations of spike protein. The experiment involves recording I_{ds} continuously in time at a fixed V_{gs} of 300 mV while injecting analytes at different times into the microfluidic chamber. The objective of this experiment is to quantify the sensitivity of this antibody-modified gFET and evaluate its limit of detection. In Fig. 3d, we show the corresponding transient response of DI_{ds}/I_0, where I_0 is the initial I_{ds} (i.e., at t = 0) and DI_{ds} is evaluated by subtracting I_0 from the subsequently recorded I_{ds}. We initially perform repeated injections of the buffer solution and monitor the gFET's DI_{ds} response. The purpose of these injections is to record possible artifacts which might contribute to a false sensor response. The sensor response due to three buffer injections are marked with yellow shading in Fig. 3d. Although each injection of the buffer solution generates a small detectable response, they are consistent among the three injections and, more critically, do not cause a permanent shift in the DI_{ds}/I_0 baseline. These observations give confidence that the artifacts of the injection process are negligible and temporary, and thus do not contribute to the steady-state sensor response due to the antibody-spike protein interactions. We then monitor the transient sensor response due to injections of the spike protein (see Methods for discussion on the concentrations). Upon each spike injection, marked with red arrows in Fig. 3d, a small bump is initially observable in the transient curve of the sensor response, associated with the artifact of the injection. However, this response is accompanied with a strong decrease in DI_{ds}/I_0, that follows an apparent exponential behavior (marked with dashed exponential fits). The subsequent spike injection occurs once DI_{ds}/I_0 establishes a new steady-state baseline. Each of the spike protein injections generates a qualitatively similar response, with increasing magnitude, as expected for increasing concentration of spike protein in the buffer solution.

Figure 3e shows the sensitivity plot of the antibody-modified gFET, plotting the sensor response (the amplitude of the exponential decay fitting function) against its corresponding spike concentration. Since the sensor response must be null when the target analyte concentration is zero, a linear fit to the data must go through the origin and we are hence able to make a meaningful fit, obtaining a sensitivity of 0.59 ± 0.04% aM. Analysis of the electronic noise in these measurements reveals a 36 nA_{rms} input-referred noise (0.3% of I_0), corresponding to an estimated limit of detection of 1.5 aM (see Supplementary Note 2).

The excellent sensitivity of these gFETs, which could be further optimized in terms of electrical characteristics, reinforces the prospects of NanoBioFETs as biosensors in experiments involving ultralow concentrations of analytes.

Sensing using aptamer-modified NanoBioFET

We next examine the versatility of the NanoBioFET platform in adapting aptamers as bioreceptors for detecting spike proteins. In recent years, aptamers have become increasingly appealing as capturing probes due to their cost-effectiveness and durability [7]. More critically, modifying FET-based sensors with aptamers has proven to be an effective strategy in significantly relaxing the requirements on λ_{Debye} and, consequently, the ionic strength of the sensing environment [39]. Recent demonstrations have revealed the utility of aptamer-modified FET sensors in detecting analytes at physiological ionic strength [8], which has a λ_{Debye} of 0.7 nm. The sensing mechanism of an aptamer-modified FET-based sensor is attributed to the fact that the analyte-induced conformational changes of the aptamer alter the surface charge within λ_{Debye}, generating a detectable electronic signal. In our experiments, explained below, we demonstrate the successful electronic detection of spike proteins in buffers solutions having a λ_{Debye} of ~ 2 nm.

We implement aptamer-modified gFETs following an identical tSPL fabrication and biofunctionalization procedure as in the experiments in Figs. 1 and 2, and we use a biotinylated anti-SARS-CoV-2 aptamer as bioreceptor (see Methods for details). Before the electrical sensing experiments, we employ fluorescent microscopy to confirm the aptamer attachment in the channel region of the gFETs designated as biosensors. Indeed, the strong fluorescence in the channel region of an aptamer-modified gFET (see left panel in Fig. 4b) confirms the effectiveness of our procedure in locally attaching aptamers. In this experiment, we also demonstrate the versatility of this approach in implementing control gFETs on the same chip by leveraging the spatial-selective biofunctionalization capability of tSPL. Control devices are produced simply by skipping the tSPL step in the channel region of a few select gFETs, while subjecting these gFETs to the same subsequent surface chemistry treatments as sensor gFETs. The fluorescent microscopy results for the control gFET (see right panel in Fig. 4b) confirm the chemical inactivity of the channel region in the control gFET with minimal non-specific binding.

In Fig. 4c, we present SPR experiments confirming the binding between the anti-SARS-CoV-2 aptamer and spike protein in 0.1X PBS, corresponding to a λ_{Debye} of approximately 2 nm. The subsequent electronic sensing experiments in a microfluidic chamber demonstrate the ability of aptamer-modified gFETs in generating detectable electronic signals in response to spike protein injections in the same buffer concentrations (see Fig. 4d). The simultaneous monitoring of an adjacent control device in this experiment provides confidence about the fidelity of the electronic signals generated by the gFET biosensor. This key feature of the NanoBioFET platform in enabling differential detection and simultaneous monitoring of non-specific binding is an important step toward achieving robust analyte detection using FET-based biosensors.

A closer look at the results in Fig. 4d reveals two important observations. The first observation is the significantly weaker signal amplitude of the aptamer-modified gFET compared to its antibody-modified counterpart in Fig. 3d. Whereas the antibody-modified gFET generates a DI_{ds}/I_0 of 2.5% in response to 5 aM of spike concentration, the aptamer-modified counterpart produces an order of magnitude weaker signal amplitude when exposed to 500 aM of spike protein. We attribute this characteristic primarily to the significantly smaller λ_{Debye} at 0.1X PBS. We expect that ongoing research in the field, focused on increasing the λ_{Debye} at a given ionic strength [36] and developing alternative chemical conjugation strategies beyond biotin-streptavidin will directly benefit future experiments utilizing aptamer-modified gFETs. The second observation pertains to the relationship between the signal amplitude and the spike protein concentration. The data indicate a nearly diminishing response with the subsequent spike protein injections at higher concentrations. This observation suggests that the capturing aptamers on the gFET are reaching full occupancy, wherein the captured surface proteins block the interactions of incoming proteins with the surface probes.

Evaluation of NanoBioFET platform using live human viral particles

Following the success of spike protein detection with bioreceptor-modified gFETs, we perform a final test with human live SARS-CoV-2 viral particles and the SARS-CoV-2 antibody as bioreceptor from earlier, evaluating sensitivity to low viral loads and selectivity of the response to specific viruses. Additionally, the experiments in Fig. 3 confirm the high sensitivity of antibody-modified gFETs in detecting low concentrations of spike proteins. Therefore, we employ the antibody-modified NanoBioFET platform in experiments involving live viral particle detection.

The measurement setup and procedure are nearly identical to that for the antibody–spike protein measurements earlier, with a 1 mM HEPES buffer (see Fig. 5a and Methods for details). We monitor the temporal changes in I_{ds} during the course of the sensing experiment. The experimental sensing procedure involves injection of the blank virus medium at the beginning of the experiments, followed by a few alternating injections of SARS-CoV-2 virus and the human H1N1 influenza virus (see Methods for details on these viruses). Figure 5b shows the transient response of the antibody-modified gFET with live virus injections in 1mM HEPES. Injections of virus medium (black circle), SARS-CoV-2 virus (red diamond), and H1N1 virus (green star) are marked in Fig. 5b. The data demonstrate the sensitive and selective detection by the SARS-CoV-2 antibody-modified gFET. The SARS-CoV-2 virus (red diamond) and H1N1 virus (green star) in Fig. 5 show that the SARS-CoV-2 virus repeatedly produces an exponential-like response in the sensor, whereas the H1N1 virus (which we use as a negative control) or buffer produce no response. The first four virus injections are at a concentration of 20 $TCID_{50}$/ml and the last at 200 $TCID_{50}$/ml, estimated to be about 10 infectious virus particles per ml, demonstrating ultra-sensitive detection of the live virus. The insensitivity of the sensor to H1N1 injections highlights the selectivity of the platform.

Conclusions

In conclusion, the results presented here establish a paradigm shift in functionalization of FETs for biosensing. While so far functionalization of FET based biosensors is achieved by drop casting without any spatial selectivity, here we show a scalable CMOS compatible surface functionalization nanofabrication strategy that allows modification of individual FETs on the same chip with distinct pathogen-specific bioreceptors, with nanoscale resolution. We call this biosensor chip NanoBioFET platform. The NanoBioFET platform is implemented through the combination of thermal scanning probe lithography, thermochemically sensitive polymers which are spin-coated on the FETs chip, and *in-situ* thermal imaging. We demonstrate that this methodology can be used to chemically functionalize individual FETs with different bioreceptors at sub-20 nm resolution and 200 nm pitch, a distance comparable to the pitch of modern FETs array in CMOS chip. Functionalization of target regions with sub-micron pitch is a crucial ingredient to achieve massively parallel FET detection of multiple target pathogens. The ability to pattern individual FET also allows for *in-situ* differential sensing, a key feature to ensure signal fidelity.

The versatility of NanoBioFET is demonstrated by modifying gFET chips with antibody and aptamer bioreceptors and subsequently employing them in electronic detection of spike protein and human SARS-Cov-2 live virus. The polymer film covering the FET allows nano-functionalization, and it functions as a coupling capacitor between the surface-anchored bioreceptors and the buried FET sensors, allowing the electronic detection of interactions between target analytes and specific bioreceptors. The electronic sensing experiments reveal ultrasensitive and selective sensing performance of the NanoBioFET platform. We achieve robust detection for 5 aM of SARS-CoV-2 spike proteins and 10 human SARS-CoV-2 infectious live virus particles/mL, as well as selectivity against human influenza A (H1N1) live virus.

Lastly, we remark on the nanomanufacturing prospects of the proposed NanoBioFET platform. A key asset of this functionalization strategy is its generalizability to various FET materials from silicon to graphene. Indeed, the polymer stack is spin coated atop the fully fabricated chips, a process scalable to commercial silicon and other types of substrates with up to 300-mm diameter. Therefore, the NanoBioFET platform is compatible with commercial semiconductor manufacturing for producing CMOS chips that can contain many FETs (thousands to millions), where each FET or a group of FETs can be modified for detecting a specific target pathogen. To this end, we note that the tSPL process could be parallelized with the use of hot probes arrays, while the scanner head could work in parallel with picoliter piezotype printing. Finally, tSPL is a flexible and sustainable nanofabrication method that does not require vacuum or high energy or alignment marks. The multiplexed parallel sensing enabled by the NanoBioFET platform will offer unprecedent opportunities in the fields of in-home diagnostics, wearables, AI for health data, and e-health.

Methods

FET devices fabrication

The FETs are fabricated using a four-stage process. The first stage involves the preparation of the substrate and graphene material. The substrate is prepared by covering SiO_2-coated silicon substrates with a 10-nm aluminum oxide (Al_2O_3) film grown by atomic layer deposition at 270°C, followed by the densification of Al_2O_3 at 500°C for 1 hour in an oxygen ambient. Commercially available single layer graphene films (ACS Material), grown by chemical vapor deposition (CVD) on copper metal substrates, are then transferred on the Al_2O_3-coated substrates using a standard PMMA-based transfer method [40] (details in Supplementary Note 3). In the second stage, graphene islands constituting the channel region of FETs are patterned using a combination of electron beam lithography (EBL) and plasma cleaning (details in Supplementary Note 3). In the third stage, fabrication of gFET array is complete through the formation of source and drain metal electrodes using a combination of EBL patterning, e-beam evaporation of 5 nm Cr/ 20 nm Ti/ 25 nm Au metal stack, and lift-off in acetone, followed by covering the metal electrodes with an EBL-patterned SU8 isolation film. Stable connections are made from the contact pads to external test circuit using spring loaded pogo pins. The contact pads are designed to lie outside the microfluidic chamber during electrical measurements and allow space for the pogo pins.

Polymer synthesis

A solution of (E)-3-(4-(3-methoxy-3-oxoprop-1-en-1-yl)phenoxy)propyl methacrylate (Mcoum), 2-((((tetrahydro-2H-pyran-2-yl)oxy)carbonyl)amino)ethyl methacrylate (Mcarb), and azobisisobutyronitrile (AIBN) is prepared in THF in a glovebox (Mcoum:Mcarb:AIBN = 40:160:1). This solution is stirred at 70 ºC in the glovebox for 16 hours, after which, the solution is exposed to air and purified by adding dichloromethane, precipitating from cold hexanes, filtering, and drying under vacuum to isolate poly((tetrahydropyran-2-yl-N-(2-methacryloxyethyl)carbamate)-co-(methyl-4-(3-methacryloyloxypropoxy)cinnamate)) (PMCC) as a white solid (see Fig. 1b). More information are reported in [25–29]. The purity is determined via 1H nuclear magnetic resonance spectroscopy.

Two-polymer resist stack

The two-polymer resist stack is spin coated on the desired chip in a two-step process. First, a PMCC film (about 70 nm thick) is spin-coated on the chip. The PMCC film is obtained by using a 15 mg/ml solution of PMCC dissolved in cyclohexanone [28, 41]. The chips are spun at 1000 RPM for 5 seconds and 1500 RPM for 15 seconds to disperse the PMCC solution, then 4000 RPM for 30 seconds to evenly apply a thin film to the substrate. The chips are then treated with 302 nm UV light to crosslink the polymer and increase adhesion to the substrate. Second, a PPA film (10–20 nm thick) is spin coated on PMCC. PMCC coated chips are spin-coated with a solution of 0.5% PPA in anisole to cover the PMCC surface. The spin-coating of PPA is performed at 6000 RPM for 30 seconds.

Thermal Scanning Probe Lithography and Microscopy

Patterning of the PMCC/PPA polymeric stack is performed using a commercial tSPL system (NanoFrazor, Heidelberg Instruments, Germany), which utilizes a heated silicon probe [23]. For patterning, the probe on the head of the thermal cantilever is heated up by a resistive micron-heater. The probe works as a

separate thermal reading sensor for *in-situ* topography thermal imaging when the micro-heater is turned off. This is a key feature that allows imaging of the FETs underneath the polymer resist, permitting the local functionalization without the need of markers. During the patterning, the thermal reading sensor probes the topography of the patterned structure right after each patterning line when retracing back in contact mode, which leads to the simultaneous patterning and imaging capability of the NanoFrazor system as well as a closed feedback loop correction [27, 28, 41]. The probe temperature is automatically calibrated through the system software according to the current-voltage characteristics of the Si tip [42]. The tSPL patterning parameters (such as write temperature, dwell time, and load) are adjusted to achieve the amine deprotection on the PMCC surface and PPA removal, while controlling the depth of the lithographic indentation. Details on the calibration of the optimal tSPL writing temperature, load and dwell time are reported in the Supplementary Note 5.

Nanoscale local biochemical functionalization

The biotin-streptavidin interaction is used as the bio-conjugation strategy to attach ad-hoc bioreceptors in designated regions of chips. Following the tSPL patterning to expose surface amine (-NH_2) groups, the chip is covered with a solution of 100 nM NHS-Biotin in dimethyl sulfoxide (DMSO) and incubated for 1 hour. The NHS ester groups react with the surface NH_2 groups, conjugating the biotin to the surface. The chip is then washed with a 1x phosphate buffered saline solution (PBS) and DI-H_2O to remove any non-reacted material, and dried using compressed N_2 gas. The chip is then functionalized with 100 nM streptavidin in 1x PBS for 30 min. Following this step, the sample is functionalized with the desired biotinylated bioreceptor: 100 nM anti-SARS-CoV-2 antibody in 1x PBS, 100 nM anti-SARS-CoV-2 aptamer in DI water or 100 nM Influenza A anti-Hemagglutinin aptamer in DI water.

All solvents are acquired from Sigma-Aldritch, unless stated otherwise. The (+)-Biotin N-hydroxysuccinimide (NHS) ester, DyLight™-conjugated esters, streptavidin are acquired from ThermoFisher Scientific. Biotinylated Anti-SARS-CoV-2 Spike RBD Neutralizing Antibody (S1N-VM226), as well as SARS-CoV-2 spike proteins for detection are purchased from ACRO Biosystems. Aptamers are synthesized per order from Integrated DNA Technologies (IDT) using the following sequences from previous studies [43, 44]: Anti-SARS-CoV-2 Aptamer-6C3 5'-CGCAGCAC CCAAGAAC AAGGACTG CTTAGGAT TGCGATAG GTTCGG-3' (see Fig. S2) [43]. Anti-Hemagglutinin (HA) Aptamer-RHA-0006 (*Integrated DNA Technologies*, 5’-GGGTTTGG GTTGGGTT GGGTTTTT GGGTTTGG GTTGGGTT GGGAAAAA-3’, see Fig. S3) [44]. Aptamers are modified with biotin on the 5’ end and tagged with TYE™ 665 (Aptamer-6C3) or 6-Carboxyfluorescein (Aptamer-RHA-0006) fluorescent dye on the 3’ end, formulated by Integrated DNA Technologies, Inc. [8, 9] and purified using high performance liquid chromatography (HPLC) [43]. See Supplementary Note 4 for further details on the functionalization, incubation process and aptamers.

Electrical measurements

The gFET chip is placed inside a custom-made microfluidic chamber with a ~ 350 µl volume, (shown in Supplementary Figure S7) and the gFETs are then covered with a buffer solution. An Ag/AgCl reference electrode is utilized as the gate. The FET electrical response is continuously monitored by means of a custom-made Printed Circuit Board. This circuit convers the drain-source current into a voltage using a transimpedance amplifier, and subsequently, the output voltage is digitized with a data acquisition instrument (NI USB6353X series, National Instruments). A custom LabVIEW control interface is employed to operate these instruments. The transfer curve of the device is measured multiple times for reproducibility. The drain-source voltage (V_{ds}) is set to 50 mV throughout the experiments. 200 µl of buffer is placed in the microfluidic chamber at the start of the measurement. 20 µl of the analyte is injected at a concentration accounting for dilution in the chamber.

Live virus experiments

Viral stocks have been prepared ahead of the experiments conducted in the ViroStatics facility in Alghero, Italy, within a Biosafety Level 3 Laboratory. A VERO E6 cell line (Cercopithecus aethiops, kidney) was purchased from American Type Culture Collection (ATCC) and was cultured in Dulbecco's modified Eagle's medium (DMEM, https://biowest.net/wp-content/uploads/2022/08/DMEM-High-Glucose.pdf) supplemented with 10% fetal bovine serum (FBS) (Biowest), 1% antibiotic solution penicillin/streptomycin (Biowest), 1% L- glutamine (Biowest), i.e., complete medium, at 37°C with 5% CO_2. Human 2019-nCoV strain 2019- nCoV/Italy-INMI1, isolated in Italy (ex-China) from a sample collected on January 29, 2020, was provided by the Istituto Lazzaro Spallanzani, Rome, Italy (Archive E, "Human 2019-nCoV strain 2019- nCoV/Italy-INMI1, clade V" 2020, available online at https://www.european-virus-archive.com/virus/human-2019-ncov-strain-2019-ncovitaly-inmi1-clade-v). The virus was propagated in Vero E6 cells as described above to obtain high titer virus (> 10E + 06 TCID50/mL) and was stored in DMEM 2% FBS at -80° C until use. Tissue culture infectious dose (TCID50) is defined as the dilution of a virus required to infect 50% of a given cell culture.

Similarly, a high titer (> 10E + 06 TCID50/mL) viral suspension of H1N1 (A/PR/8/34) was produced from infected cultured of MDCK (Madin-Darby canine kidney). DMEM 2% FBS was used to store the virus at -80°C. Live virus suspensions for the gFETs experiments are prepared using a buffer containing 1 mM HEPES and 0.6 mM NaCl.

SPR experiments

Putative interactions between probes and target analytes are confirmed using a 2-Channel Surface Plasmon Resonance System (Reichert® 2SPR, Reichert Inc, NY). SPR system is equilibrated with the target buffer system and all the subsequent probes, analyte samples, and blank samples are produced with the same buffer. Biotin-conjugated aptamers (IDT Corporation, IA) and antibodies (Acro Biosystems, DE) are used as probes (100 µL injection, 100 nM) and immobilized onto streptavidin-coated gold chips (Reichert Inc). Only the left channel is functionalized with the probe while the right channel is used as a reference. Analyte interactions is assessed by flowing through (25 µL/min) solutions of target analyte

samples SAR Cov-19 spike protein (Acro Biosystems) and live Covid particle (patient nasal swabs) with increasing concentrations through both channels. All experiments are run at 37°C.

Fluorescence microscopy

Figures 1d-f are taken using a Zeiss LSM 880 Airyscan Fast Live Cell confocal microscopy unit, Plan Apo 40x/1.2 Type W Oil objective and submersion, and the HeNe 633 nm laser line. Figure 2b, c, d, f fluorescence imaging is done using a Nikon Ti2-E Motorized Microscope equipped with a 7-line solid state light source, CFI60 Plan Apochromat Lambda 10x and 40x lenses and ORCA-Fusion Gen-III sCMOS camera.

Declarations

Acknowledgements

This work is supported by funding from Lendlease LLC and Mirimus Inc. The device fabrication was done in part at the Nanofabrication Facility at the Advanced Science Research Center at The Graduate Center of the City University of New York, and in part at the Nanofabrication Cleanroom Facility at the NYU Tandon School of Engineering. E.R. and D.S. thank Dr. Alberto Sangiovanni-Vincentelli, Dr. Nathalie Pinkerton and Dr. Paramjit Arora for the useful discussions.

References

1. Bergveld, P., *Development, Operation, and Application of the Ion-Sensitive Field-Effect Transistor as a Tool for Electrophysiology*. IEEE Transactions on Biomedical Engineering, 1972. BME-19(5): p. 342–351.
2. Bergveld, P., *Thirty years of ISFETOLOGY: What happened in the past 30 years and what may happen in the next 30 years*. Sensors and Actuators B: Chemical, 2003. 88(1): p. 1–20.
3. Wu, T., et al., *Experimental study of the detection limit in dual-gate biosensors using ultrathin silicon transistors*. ACS nano, 2017. 11(7): p. 7142–7147.
4. Rothberg, J.M., et al., *An integrated semiconductor device enabling non-optical genome sequencing*. Nature, 2011. 475(7356): p. 348–352.
5. Dai, C., et al., *Ultraprecise antigen 10-in-1 pool testing by multiantibodies transistor assay*. Journal of the American Chemical Society, 2021. 143(47): p. 19794–19801.
6. Seo, G., et al., *Rapid detection of COVID-19 causative virus (SARS-CoV-2) in human nasopharyngeal swab specimens using field-effect transistor-based biosensor*. ACS nano, 2020. 14(4): p. 5135–5142.
7. Nakatsuka, N., et al., *Aptamer–field-effect transistors overcome Debye length limitations for small-molecule sensing*. Science, 2018. 362(6412): p. 319–324.
8. Wu, G., et al., *Implantable aptamer-graphene microtransistors for real-time monitoring of neurochemical release in vivo*. Nano letters, 2022. 22(9): p. 3668–3677.

9. Duan, X., et al., *Quantification of the affinities and kinetics of protein interactions using silicon nanowire biosensors*. Nature nanotechnology, 2012. 7(6): p. 401–407.
10. Zhang, H., et al., *Design and fabrication of silicon nanowire-based biosensors with integration of critical factors: toward ultrasensitive specific detection of biomolecules*. ACS Applied Materials & Interfaces, 2020. 12(46): p. 51808–51819.
11. Hajian, R., et al., *Detection of unamplified target genes via CRISPR–Cas9 immobilized on a graphene field-effect transistor*. Nature biomedical engineering, 2019. 3(6): p. 427–437.
12. Kumar, N., et al., *Graphene Field Effect Biosensor for Concurrent and Specific Detection of SARS-CoV-2 and Influenza*. ACS nano, 2023. 17(18): p. 18629–18640.
13. Scotto, J., et al., *Using Graphene Field-Effect Transistors for Real-Time Monitoring of Dynamic Processes at Sensing Interfaces. Benchmarking Performance against Surface Plasmon Resonance*. ACS Applied Electronic Materials, 2022. 4(8): p. 3988–3996.
14. Cretich, M., et al., *Protein and peptide arrays: recent trends and new directions*. Biomolecular engineering, 2006. 23(2–3): p. 77–88.
15. Janasek, D., J. Franzke, and A. Manz, *Scaling and the design of miniaturized chemical-analysis systems*. Nature, 2006. 442(7101): p. 374–380.
16. Dawson, E.D., et al., *Identification of A/H5N1 influenza viruses using a single gene diagnostic microarray*. Analytical Chemistry, 2007. 79(1): p. 378–384.
17. Ligler, F.S. and J.S. Erickson, Diagnosis on disc. Nature, 2006. 440(7081): p. 159–160.
18. Rusling, J.F., et al., *Measurement of biomarker proteins for point-of-care early detection and monitoring of cancer*. Analyst, 2010. 135(10): p. 2496–2511.
19. To, K.K.-W., et al., *Temporal profiles of viral load in posterior oropharyngeal saliva samples and serum antibody responses during infection by SARS-CoV-2: an observational cohort study*. The Lancet infectious diseases, 2020. 20(5): p. 565–574.
20. Sun, J. and Y. Liu, *Matrix effect study and immunoassay detection using electrolyte-gated graphene biosensor*. Micromachines, 2018. 9(4): p. 142.
21. McKenzie, J., *The price of Moore's law*. Physics World, 2023. 36(8): p. 30.
22. Béraud, A., et al., *Graphene field-effect transistors as bioanalytical sensors: Design, operation and performance*. Analyst, 2021. 146(2): p. 403–428.
23. Albisetti, E., et al., *Thermal scanning probe lithography*. Nature Reviews Methods Primers, 2022. 2(1): p. 32.
24. Szoszkiewicz, R., et al., *High-speed, sub-15 nm feature size thermochemical nanolithography*. Nano Letters, 2007. 7(4): p. 1064–1069.
25. Albisetti, E., et al., *Thermochemical scanning probe lithography of protein gradients at the nanoscale*. Nanotechnology, 2016. 27(31): p. 315302.
26. Liu, X., et al., *Cost and Time Effective Lithography of Reusable Millimeter Size Bone Tissue Replicas With Sub-15 nm Feature Size on A Biocompatible Polymer*. Advanced Functional Materials, 2021.

31(19): p. 2008662.

27. Liu, X.Y., et al., *Sub-10 nm Resolution Patterning of Pockets for Enzyme Immobilization with Independent Density and Quasi-3D Topography Control*. Acs Applied Materials & Interfaces, 2019. 11(44): p. 41780–41790.
28. Wang, D.B., et al., *Thermochemical Nanolithography of Multifunctional a Nanotemplates for Assembling Nano-objects*. Advanced Functional Materials, 2009. 19(23): p. 3696–3702.
29. Zanut, A., et al., *A Polymer Canvas with the Stiffness of the Bone Matrix to Study and Control Mesenchymal Stem Cell Response*. Adv Healthc Mater, 2023. 12(10): p. e2201503.
30. Kim, J.E., et al., *Highly sensitive graphene biosensor by monomolecular self-assembly of receptors on graphene surface*. Applied Physics Letters, 2017. 110(20).
31. Yeh, C.-H., et al., *High-performance and high-sensitivity applications of graphene transistors with self-assembled monolayers*. Biosensors and Bioelectronics, 2016. 77: p. 1008–1015.
32. Zheng, X., et al., *Patterning metal contacts on monolayer MoS2 with vanishing Schottky barriers using thermal nanolithography*. Nature Electronics, 2019. 2(1): p. 17–25.
33. Wang, D.B., et al., *Local wettability modification by thermochemical nanolithography with write-read-overwrite capability*. Applied Physics Letters, 2007. 91(24).
34. Hwang, M.T., et al., *Highly specific SNP detection using 2D graphene electronics and DNA strand displacement.* Proceedings of the National Academy of Sciences, 2016. 113(26): p. 7088–7093.
35. Butt, H.-J., K. Graf, and M. Kappl, *Physics and chemistry of interfaces*. 2003: John Wiley & Sons.
36. Kesler, V., B. Murmann, and H.T. Soh, *Going beyond the debye length: Overcoming charge screening limitations in next-generation bioelectronic sensors*. Acs Nano, 2020. 14(12): p. 16194–16201.
37. Zhang, Y., M. Juhas, and C.K. Kwok, *Aptamers targeting SARS-COV-2: a promising tool to fight against COVID-19*. Trends in Biotechnology, 2023. 41(4): p. 528–544.
38. Guo, Y., et al., *A SARS-CoV-2 neutralizing antibody with extensive Spike binding coverage and modified for optimal therapeutic outcomes*. Nature Communications, 2021. 12(1).
39. Zhao, C., et al., *Implantable aptamer–field-effect transistor neuroprobes for in vivo neurotransmitter monitoring*. Science Advances, 2021. 7(48): p. eabj7422.
40. Li, Y., et al., *MXene–graphene field-effect transistor sensing of influenza virus and SARS-CoV-2*. ACS omega, 2021. 6(10): p. 6643–6653.
41. Liu, X.Y., et al., *Cost and Time Effective Lithography of Reusable Millimeter Size Bone Tissue Replicas With Sub-15 nm Feature Size on A Biocompatible Polymer*. Advanced Functional Materials, 2021. 31(19).
42. Durig, U., *Fundamentals of micromechanical thermoelectric sensors*. Journal of Applied Physics, 2005. 98(4): p. 044906.
43. Sun, M., et al., *Aptamer Blocking Strategy Inhibits SARS-CoV-2 Virus Infection*. Angewandte Chemie-International Edition, 2021. 60(18): p. 10266–10272.

44. Shiratori, I., et al., *Selection of DNA aptamers that bind to influenza A viruses with high affinity and broad subtype specificity*. Biochemical and Biophysical Research Communications, 2014. 443(1): p. 37–41.

Figures

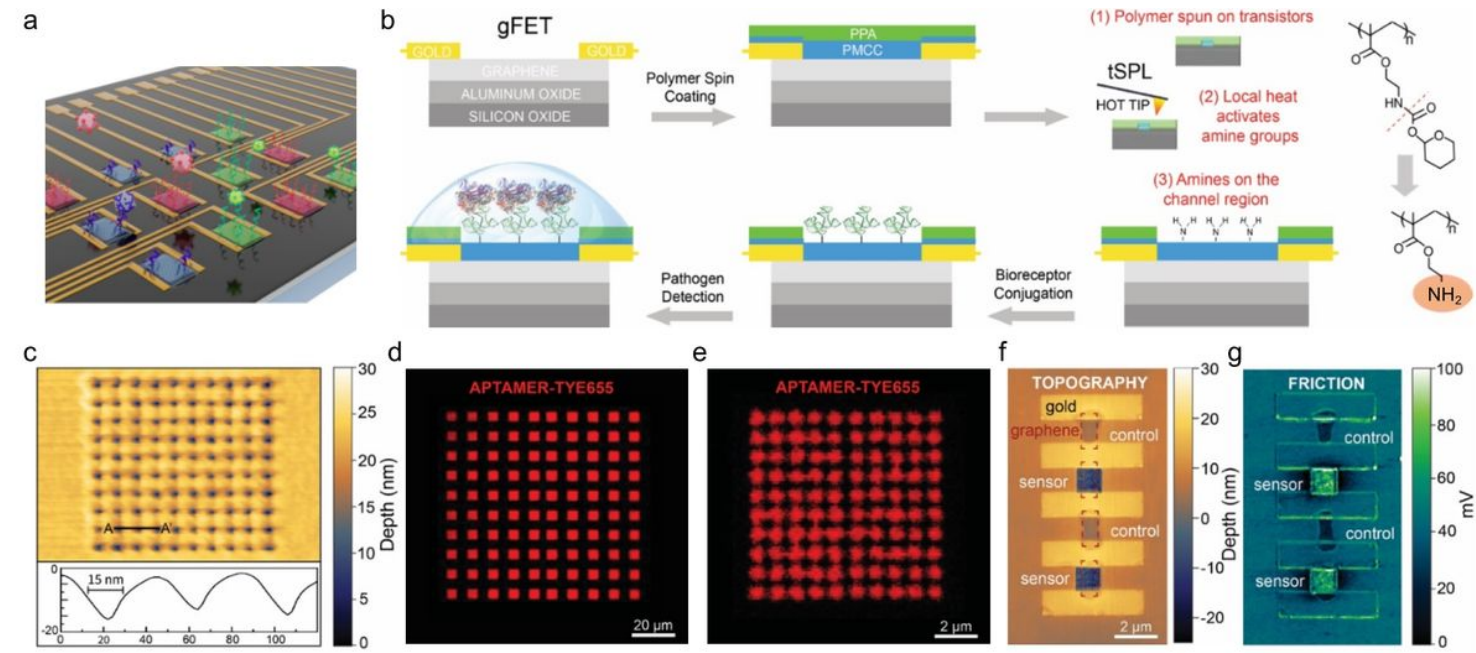

Figure 1

Sub-20 nm resolution biochemical functionalization of FETs by tSPL. **a** 3D-Render of the NanoBioFET platform for FETs based multiplexed nanoscale biosensing. **b** Schematic showing the steps of fabrication in the NanoBioFET platform, from polymer deposition onto the FETs, to tSPL nanoscale activation of amine groups, and bioreceptor bioconjugation. **c** Thermal SPM topographical image of a

tSPL nanoscale amine pattern fabricated in PPA/PMCC. In the inset, the depth profile of the corresponding cross section AA', showing a FWHM of 15 nm for each sensor pixel. **d** and **e** Fluorescence microscopy image of biotinylated aptamers terminated with a red dye on a PPA/PMCC SiO_2/Si chip. Specifically, the image shows Biotinylated Anti-SARS-CoV-2 Aptamer. After tSPL patterning, the sample is covered with a solution of 100 nM NHS-Biotin in DMSO and incubated for 1 hour. The sample is then functionalized with 100 nM streptavidin in 1x PBS for 30 min. After washing and drying, the sample is functionalized with the red-dye tagged aptamer. **f** and **g** tSPL topography (f) and friction AFM (g) images of four PPA/PMCC coated GFETs with a channel width of 1 mm, where the areas above the GFET's channel (graphene) sensors have been patterned by tSPL to remove PPA and activate amine groups on PMCC.

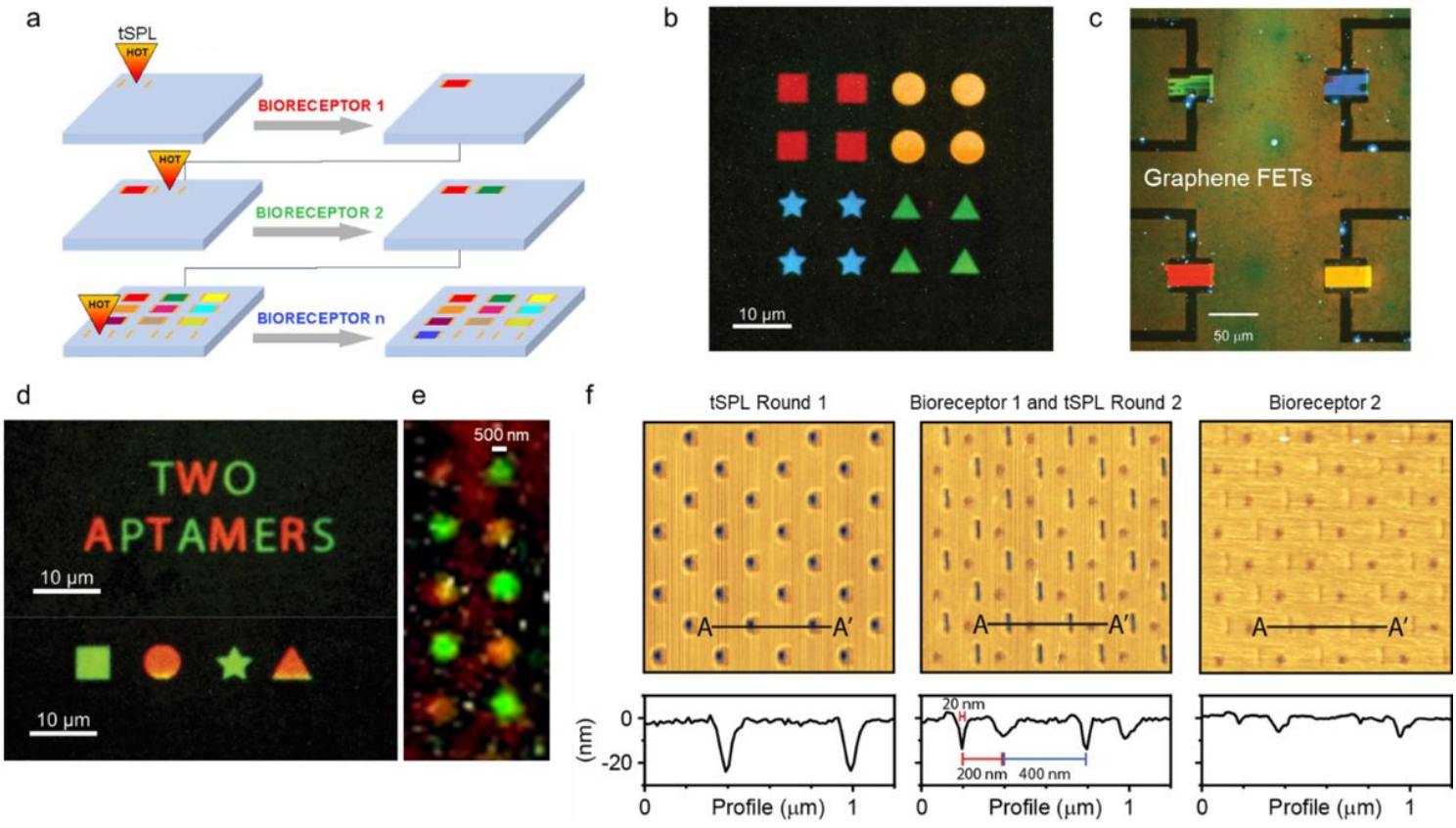

Figure 2

NanoBioFET fabrication for multiplexed nanoscale biosensing. **a** Schematics of consecutive tSPL patterning and functionalization rounds to fabricate adjacent FETs, each functionalized with a different bioreceptor for multiplexed biochemical sensing. **b** Fluorescence microscopy image of four different NHS-ester terminated dyes (red, orange, sky-blue and green) attached to amine moieties patterned by tSPL on a PPA/PMCC SiO_2/Si chip. **c** Fluorescence microscopy image of four representative graphene-based FETs functionalized with four different types of NHS-ester terminated dyes (green, sky-blue, red and orange). **d, e** Fluorescence microscopy images of two different biotinylated aptamers with terminated red and green dyes on a PPA/PMCC/SiO_2/Si chip. Specifically, the images show biotinylated anti-SARS-CoV-2 aptamer (red) and biotinylated anti-Hemagglutinin (HA) aptamer (green). The image in **e** shows a two-aptamer

pattern of 500 nm circles. **f** From left to right: first, in-situ tSPL topographical image of a matrix of circles produced after a first round of tSPL on a PPA/PMCC/SiO_2/Si chip; second, in-situ tSPL topographical image of the same area after conjugation of the surface with bioreceptor 1 (HA aptamer) using biotin/streptavidin as cross linker and after a second round of tSPL to pattern a second matrix of 20 nm dashes; third, in-situ tSPL topographical image of the same area after conjugation of bioreceptor 2 (CoV-2 aptamer) using biotin/streptavidin as cross linker. The respective cross section images show the registry and robustness of multiplexed patterning and the change in depth of the patterns after functionalization due to the filling of each pattern with the NHS-biotin/streptavidin/aptamer molecules (approximately 10 -15 nm).

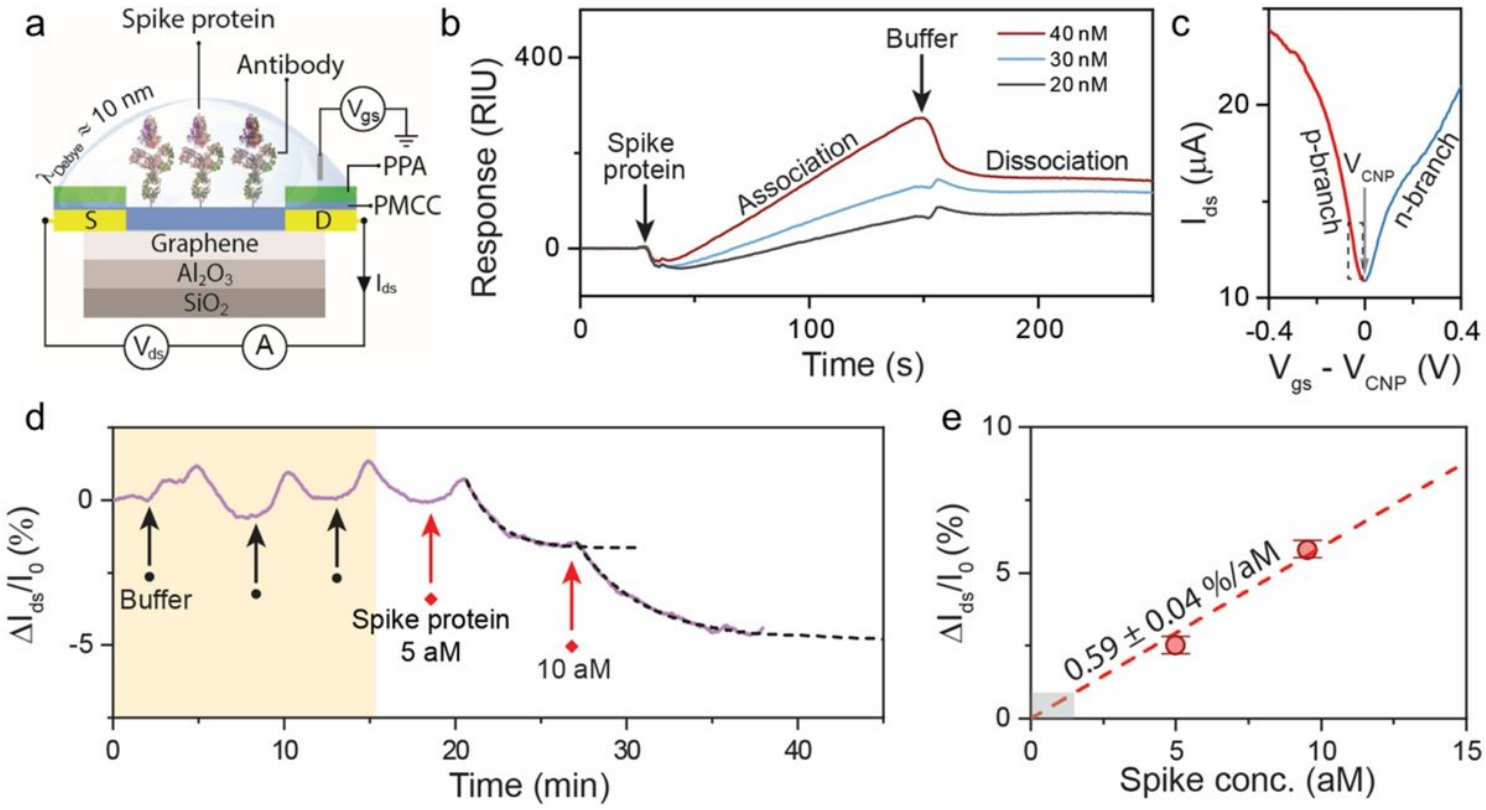

Figure 3

Spike protein–Antibody capture on the NanoBioFET platform. **a** Schematic of a gFET functionalized with SARS-CoV-2 antibody using the NanoBioFET platform. The device structure, electrical measurement setup and λ_{Debye} at 1 mM HEPES buffer are indicated. **b** SPR measurement at 1 mM HEPES buffer, demonstrating successful interaction between the antibody and spike protein. **c** Transfer characteristics of the gFET device. The p-branch and n-branch are indicated. The current and voltage range used in the transient measurement in panel d is indicated by the dashed box. **d** Transient response of the antibody-modified gFET in 1mM HEPES. Black circle and red diamond symbols denote, respectively, injections of buffer and spike protein of increasing concentrations. Dashed lines are a guide-to-the-eye of the measured signal. **e** Sensitivity plot of the gFET, obtained from a straight line fit (dashed line) to the

measured $\Delta I_{ds}/I_0$ data at different spike protein concentrations. The gray shading denotes the calculated limit of detection of the gFET, assuming a signal-to-noise ratio of 3.

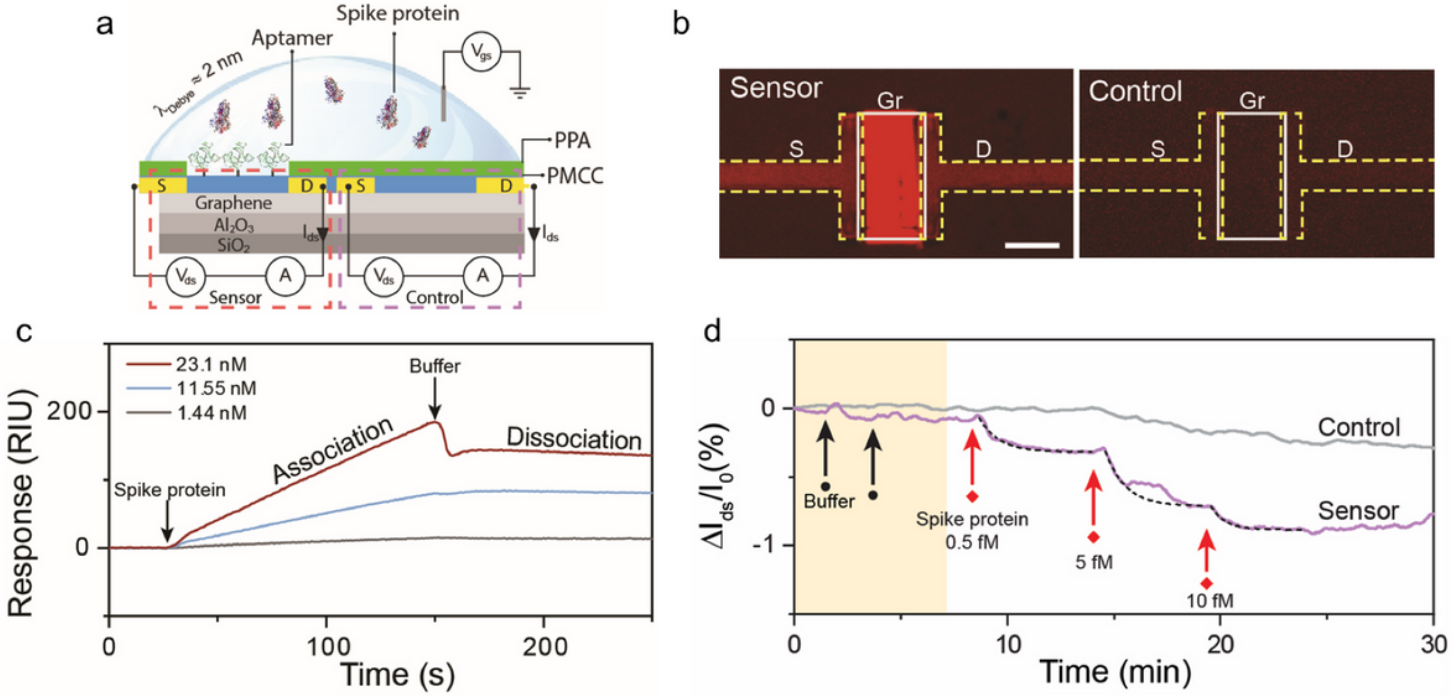

Figure 4

Spike protein–Aptamer capture on the NanoBioFET platform. **a** Schematic of a gFET functionalized with SARS-CoV-2 aptamer using the NanoBioFET platform paired with a control device. **b** Florescence microscopy of the sensor and control gFET devices, demonstrating successful immobilization of the fluorescently tagged aptamer exclusively on the sensor channel. The yellow dashed lines denote the metal electrodes of the gFET devices, and the white rectangle denotes the graphene channel. **c** SPR measurement at 0.1X PBS of binding between the aptamer and spike protein. Graphene channel is denoted with a solid box. Scale bar is 20 μm. **d** Transient responses of the aptamer-modified gFET and the adjacent control gFET in 0.1X PBS. The capability of the NanoBioFET platform in simultaneously monitoring the transient characteristics of the sensor and control gFETs gives confidence in fidelity of the detected signal by the sensor in response to the spike protein injections. Black circle and red diamond symbols denote, respectively, injections of buffer and spike protein of increasing concentrations. Dashed lines are a guide-to-the-eye of the measurement signal.

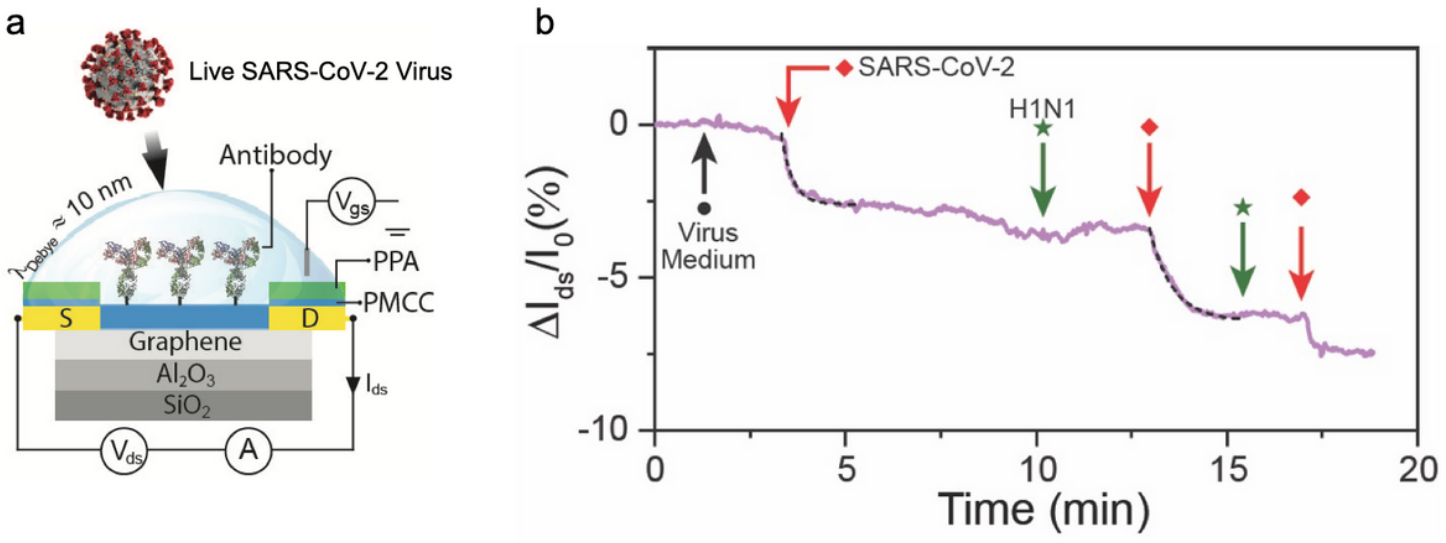

Figure 5

Ultrasensitive and selective detection of live human SARS-CoV-2 virus. **a** Schematic of a gFET functionalized with SARS-CoV-2 antibody using the NanoBioFET platform ready for detection of live SARS-CoV-2 virus. **b** Transient response of the antibody-modified gFET with live virus injections in 1mM HEPES. Injections of virus medium (black circle), SARS-CoV-2 virus (red diamond) and H1N1 virus (green star) are indicated. The first four virus injections were at a concentration of 20 $TCID_{50}$/ml and the last at 200 $TCID_{50}$/ml, estimated to be of the order of 10 live particles in the measurement volume, demonstrating ultra-sensitive detection of the live virus. The insensitivity of the sensor to H1N1 injections highlights the selectivity of the platform. Dashed lines are a guide-to-the-eye of the measurement signal.

Supplementary Files

This is a list of supplementary files associated with this preprint. Click to download.

- SupplementaryInformationDec26.docx